CrossMark

RESEARCH PAPER

Characterizing the performance of the hydrodynamic trap using a control-based approach

**Anish Shenoy · Melikhan Tanyeri ·
Charles M. Schroeder**

Abstract Hydrodynamic trapping allows for the confinement and manipulation of small objects in free solution, away from solid boundaries and without the need for optical or magnetic fields. In order to achieve robust trapping over long time scales, it is imperative to evaluate trap performance using different control schemes and to understand the effect of system parameters on trap stability. In this work, we investigate the performance of a hydrodynamic trap actuated by varying combinations of proportion-integral-derivative controllers. We further develop a control-based model of the trap, and we characterize trap performance for a wide range of particle Peclet numbers and response times. Overall, an increased understanding of trap performance will facilitate the design of improved controllers to enable robust trapping under variable system parameters.

A. Shenoy
Department of Mechanical Science and Engineering, University of Illinois at Urbana-Champaign, Urbana, IL 61801, USA

M. Tanyeri · C. M. Schroeder (✉)
Department of Chemical and Biomolecular Engineering, University of Illinois at Urbana-Champaign, Urbana, IL 61801, USA
e-mail: cms@illinois.edu

C. M. Schroeder
Center for Biophysics and Computational Biology, University of Illinois at Urbana-Champaign, Urbana, IL 61801, USA

1 Introduction

The development of techniques for trapping and precisely manipulating single particles and molecules has catalyzed a revolution in diverse fields ranging from biology to soft condensed matter physics. For example, these techniques have been used for cellular chromosome manipulation (Vorobjev et al. 1993; Harsono et al. 2013), manufacturing 2D and 3D nanostructures (Castelino et al. 2005), nanopatterning (Mcleod and Arnold 2008; Tsai et al. 2012), and for studying non-equilibrium statistical mechanics (Reimann 2002). To this end, a wide variety of techniques have been developed and extensively studied, including those based on optical fields (Ashkin et al. 1986; Grier 2003; Neuman and Block 2004; Righini et al. 2008; Yang et al. 2009; Roxworthy et al. 2012), magnetic fields (Gosse and Croquette 2002; Lee et al. 2004; Mirowski et al. 2005), microvortices (Lutz et al. 2006; Lin et al. 2008; Petit et al. 2012), and electrical fields (Cohen and Moerner 2005, 2006, 2008; Armani et al. 2006; Cummins et al. 2013).

Trapping techniques can be broadly classified into passive and active trapping schemes. Passive techniques confine particles by generating a local minimum in a potential energy profile (i.e., a potential well) around the target particle position. This potential energy minimum serves as an attractive point for a particle. For passive traps, feedback control is generally not required to stabilize a trapped particle, because the depth of the potential well can be tuned to mitigate particle fluctuations due to thermal and environmental noise. Passive techniques include optical traps (Grier 2003; Neuman and Block 2004; Chiou et al. 2005; Yang et al. 2009; Dholakia and Čižmár 2011), magnetic traps (Gosse and Croquette 2002; Lee et al. 2004; Mirowski et al. 2005), streaming microvortices or microeddies (Lutz et al. 2006; Lin et al. 2008; Petit et al. 2012),

and plasmonic traps (Pelton et al. 2006; Righini et al. 2008; Juan et al. 2011; Roxworthy et al. 2012).

Active traps, on the other hand, require feedback to achieve particle confinement at a desired set point. In active traps, feedback control can be used to correct for thermal fluctuations of a particle in an otherwise stable environment or to stabilize a particle in a semi-stable potential energy profile. In the first category, electric field-based traps (Cohen and Moerner 2005, 2006; Armani et al. 2006; Cohen and Moerner 2008; Cummins et al. 2013) utilize electrokinetic flow-induced drift velocity to correct a particle's position due to thermal fluctuations. The hydrodynamic trap (Tanyeri et al. 2010, 2011a; Tanyeri and Schroeder 2013) is an example of the second category, wherein a particle is confined at a semi-stable equilibrium point in fluid flow. In this case, feedback control (using a simple P controller at a minimum) is necessary to stabilize a particle at a desired point. Other examples of feedback-assisted trapping platforms include the macroscopic four-roll mill (Bentley and Leal 1986) and the planar extensional cross-slot flow device (Schroeder et al. 2003, 2004), in which the stagnation point was manipulated by manually varying the relative pressure difference between the two outlet channels by changing the hydrostatic pressure of one outlet stream.

Recently, we showed that hydrodynamic trapping enables the precise 2D positioning and manipulation of micro and nanoscale particles using the sole action of fluidic forces, and we have demonstrated confinement of a 500-nm-diameter particle to within ~0.18 µm of the set point position (Tanyeri and Schroeder 2013). In prior versions of the hydrodynamic trap, we employed linear feedback controllers without a systematic study of the control scheme, gain constants, or system parameters. However,

robust confinement of particles over long time scales critically requires a clear understanding of the effect of the controller and system parameters on the stability of trapped particles. For example, in the macroscopic computer-controlled four-roll mill, it was reported that trapping was difficult, if not impossible to achieve, using P and PD control, owing to slow response times of the fluid and the measurement delay.

In this work, we implement three different control schemes for hydrodynamic trapping, including a proportional (P), a proportional-integral (PI), and a proportional-derivative (PD) controller. We study the effect of controller gain constants on the stability of trapped particles. In addition, we develop a control-based model to characterize the response of the hydrodynamic trap, and we use this model to simulate the stability of trapped particles over a wide range of response times and Peclet numbers. In this way, we use a combination of experiments and simulations to provide a clear understanding of the effect of feedback controllers and system parameters on trap performance, which will facilitate the development of improved controllers for robust trapping under variable system conditions.

1.1 Hydrodynamic trap: trapping mechanism

The hydrodynamic trap is based on the active feedback control of a stagnation point flow generated at the cross-slot junction of a two-layer PDMS-based microfluidic device (Fig. 1). In the fluidic layer, fluid enters the cross-slot through two opposing inlet streams and exits through two perpendicular outlet streams, as shown in Fig. 1b. A control layer is positioned above the fluidic layer and consists of a pneumatic valve situated above one of the outlet
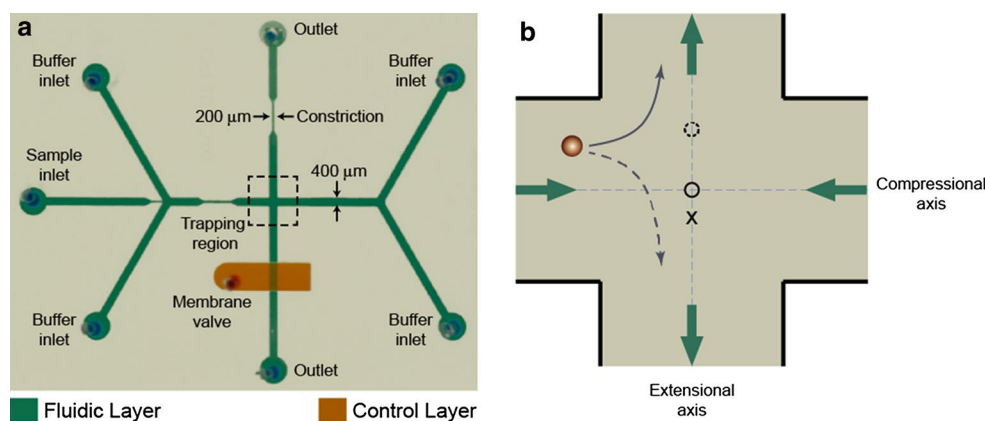

Fig. 1 Microfluidic-based hydrodynamic trap. **a** Optical micrograph of the device. Particles are confined at a user-defined set point in the cross-slot junction (indicated by the *dashed box*). **b** Schematic of the cross-slot region and trap mechanism. Two inlet and two outlet streams are indicated by the *thick arrows* (*green*), × indicates the user-defined set point, the *solid circle* indicates the initial stagnation point position, and the *solid arrow* indicates the particle trajectory. To trap the particle, the stagnation point is translated along the extensional axis to a new position (shown by the *dashed circle*), which directs the particle toward the set point along a new trajectory (indicated by the *dashed arrow*). The origin is at the center of the cross-slot (color figure online)

streams. Control is achieved by the actuation of the integrated membrane valve on the device. In this setup, the flow field in the cross-slot consists of a compressional axis along the inlet direction and an extensional axis along the outlet direction, with no rotational flow characteristics. This flow pattern is known as a planar extensional flow and contains a stagnation point (a point with zero velocity) in the cross-slot region. The local fluid velocity in the vicinity of the stagnation point depends on the relative distance from the stagnation point, so we can express the velocity at a point as a superposition of velocities along the extensional and compressional flow directions:

$$\vec{v}(x, y) = \vec{v}_{ext}(y) + \vec{v}_{comp}(x)$$
$$\vec{v}_{ext}(y) = \dot{\varepsilon}(y - y_s)\hat{j} \qquad (1)$$
$$\vec{v}_{comp}(x) = -\dot{\varepsilon}(x - x_s)\hat{i}$$

where $\hat{i}$ and $\hat{j}$ are unit vectors along the compressional and extensional axes, respectively, $\dot{\varepsilon}$ is the strain rate, and (x_s, y_s) is the stagnation point position. The flow field is characterized by a set of hyperbolic streamlines within the cross-slot junction.

From the velocity field, it can be inferred that a particle is attracted toward the stagnation point along the compressional axis and repelled from the stagnation point along the extensional axis. In this work, we consider 1D particle trapping at arbitrary points along the principal axis of extension in planar extensional flow; in other words, we characterize trap stability along the unstable trapping direction (outflow direction). Due to the semi-stable nature of the trap potential, particles are stably confined along the compressional flow axis without the need for active feedback control in this direction. Therefore, the stagnation point is a stable equilibrium point along the compressional axis and an unstable equilibrium position along the extensional axis. From this view, it is clear that feedback control is necessary for particle trapping—for instance, in directing a particle toward the stagnation point in the y-direction. Following the initial trapping phase, further disturbances due to Brownian motion and environmental noise necessitate the use of active feedback control for particle confinement.

The mechanism of hydrodynamic trapping has been previously described (Tanyeri et al. 2010, 2011a; Tanyeri and Schroeder 2013); here, we briefly review it for clarity. Consider a freely suspended particle entering the cross-slot junction (Fig. 1b) that is to be trapped at a user-defined set point (indicated by the 'x' symbol). Without control, the particle would simply follow the trajectory (streamline) shown by the solid arrow. In order to trap the particle, the controller moves the stagnation point in the positive y-direction instantaneously, which would tend to direct the particle to follow a new trajectory (shown by the dashed line) that will cause it to approach the set point. Next, the

updated position of the particle is acquired, and the process is repeated, continuously moving the stagnation point position along the extensional axis within the cross-slot.

The motion of the stagnation point is achieved by pressurization or de-pressurization of the integrated membrane valve (Fig. 1a). The movement of the valve enables a dynamic metering of the flow rate in the fluidic channel in the lower outlet stream. In this way, pressurizing the valve causes a constriction of the outlet channel under the valve, which increases the fluidic resistance, consequently decreasing fluid flow through the lower outlet channel and moving the stagnation point toward this channel. De-pressurization causes an analogous effect in the upper outlet flow channel. The overall control process consists of the following steps and is implemented using a LabVIEW program: (1) determining the centroid position of the particle by performing image acquisition and analysis of the camera feedback data, (2) calculating the offset error between the set point position and current position, and (3) translating the stagnation point in the +y-direction (or −y-direction) by de-pressurizing (or pressurizing) the valve using the control algorithm described in the Methods section. This process is analogous to the balancing of a pendulum in an inverted position, which is an unstable equilibrium point.

1.2 Hydrodynamic trap: control model

As discussed previously, hydrodynamic traps based on cross-slot microfluidic devices require feedback control only for manipulating the position of a particle in the y-direction (along the extensional axis). Hence, we focus on developing a control model for only the y-direction, because the x-direction (compressional flow axis) is intrinsically stable. Given a stagnation point position y_s, the velocity of a particle in the y-direction is given by:

$$\frac{dy}{dt} = \dot{\varepsilon}(y - y_s) \qquad (2)$$

where $\dot{\varepsilon}$ is the strain rate, y is the particle position, and y_s is the current stagnation point position, where all positions are measured along the extensional axis.

There is a finite delay between setting a new stagnation point position on the computer versus the actual updating of the stagnation point position via valve actuation on the microdevice. The movement of the stagnation point from its prior position to the new position can be modeled as a first-order process:

$$\frac{dy_s}{dt} = \frac{1}{t_v}\left(y_{s,new} - y_s\right) \qquad (3)$$

where $y_{s,new}$ is the new stagnation point position set by the controller and t_v is the system response time. Together, Eqs. (2) and (3) represent the uncontrolled system.

In this process, there is a second finite delay in acquiring and analyzing image data to determine a particle's position, which is defined as the measurement delay, t_m. Furthermore, the stagnation point has a limited range of movement due to physical constraints on the on-chip membrane valve, which is accounted for in the model. Finally, the particle's final position y_f is also influenced by Brownian motion, which can be modeled as:

$$y_f = y + y_b \tag{4}$$

Here, y_b is the magnitude of random thermal motion superposed on the mean flow position y at a single time step. Following the fluctuation–dissipation theorem, y_b is assumed to be a Gaussian-distributed random variable with zero mean value and a standard deviation given by:

$$y_{b,std} = \sqrt{\frac{2k_b T}{3\pi \eta d}(t_m + t_v)} \tag{5}$$

where k_b is the Boltzmann constant, T is the absolute temperature, η is the viscosity, and d is the particle diameter. Also, t_m and t_v are the measurement delay and the system response times, respectively. The time scale in Eq. (5) results from the implementation of the control algorithm for trapping a particle of diameter d. In particular, the Lab-VIEW algorithm initiates the control process (characteristic time t_v), after which the camera and imaging process determine the new position of the particle (characteristic time t_m). Thus, between successive snapshots of a particle's position, a time equal to $(t_v + t_m)$ has elapsed, as shown in Eq. (5).

Following acquisition of an image and determination of particle position from image data, the error between the set point and the current particle position is calculated. The error is input to the controller, which outputs a control signal to the system. The relationship between the input and the output of the controller is:

$$Q = \underbrace{K_p P}_{\text{Proportional}} + \underbrace{K_i \int_0^t P dt}_{\text{Integral}} + \underbrace{K_d \frac{dP}{dt}}_{\text{Derivative}} \tag{6}$$

where P is the input and Q is the output. In the case of the control model, P is the offset error (distance) and Q is the position of the new stagnation point. In experiments, P is the offset error (distance) and Q is voltage applied to the pressure transducer controlling the on-chip membrane valve, though it should be noted that the experimental controller does not use the exact form described in Eq. (6) (refer to the Supplementary Information for additional details). In Eq. (6), K_p is the proportional gain constant, K_i is the integral gain constant, and K_d is the derivative gain constant. For implementing a proportional-only (P)

controller, K_i and K_d are set to zero, for a proportional-integral (PI) controller, K_d is set to zero, and finally for a proportional-derivative (PD) controller, K_i is set to zero.

To facilitate analysis, parameters are converted to dimensionless forms by choosing the particle diameter d and the diffusion time $t_{diff} = \frac{3\pi \eta d^3}{4k_b T}$ as the characteristic length and time scales, respectively. In this way, dimensionless parameters are denoted by variables with over-bars and defined in the following way:

$$\bar{y} = \frac{y}{d}, \quad \bar{y}_s = \frac{y_s}{d}, \quad \bar{y}_{s,new} = \frac{y_{s,new}}{d},$$
$$\bar{t} = \frac{t}{t_{diff}}, \quad \tau_v = \frac{t_v}{t_{diff}}, \quad \tau_m = \frac{t_m}{t_{diff}}$$

The particle Peclet number Pe is defined as the ratio of the diffusive time scale of the particle t_{diff} to the convective time scale $\dot{\varepsilon}^{-1}$:

$$Pe = \frac{t_{diff}}{t_{conv}} = \frac{3\pi \eta \dot{\varepsilon} d^3}{4k_b T} \tag{7}$$

Using the characteristic length and time scales, Eqs. (2), (3), and (5) are recast in dimensionless form:

$$\frac{d\bar{y}}{d\bar{t}} = Pe(\bar{y} - \bar{y}_s) \tag{8}$$

$$\frac{d\bar{y}_s}{d\bar{t}} = \frac{1}{\tau_v}(\bar{y}_{s,new} - \bar{y}_s) \tag{9}$$

$$\bar{y}_{b,std} = \sqrt{\frac{\tau_m + \tau_v}{2}} \tag{10}$$

where τ_m and τ_v are the dimensionless system response time and measurement delay.

To facilitate a control-based analysis of system response, we use Laplace transforms of the above equations to define transfer functions, assuming zero initial conditions. For Eqs. (8) and (9), the transfer functions are:

$$\frac{Y(s)}{W(s)} = G_p = \frac{Pe}{Pe - s}$$
$$\frac{W(s)}{Z(s)} = G_v = \frac{1}{\tau_v s + 1} \tag{11}$$

where s is the Laplace domain variable and $W(s)$ and $Z(s)$ are the Laplace transforms of $\bar{y}_s$ and $\bar{y}_{s,new}$, respectively. If $P(s)$ and $Q(s)$ are the input and output quantities, then transfer functions for the time delay and the controller are given by the following equations:

$$\frac{Q(s)}{P(s)} = e^{-s\tau_m} \tag{12}$$

$$\frac{Q(s)}{P(s)} = K_p + \frac{1}{s}(K_i t_{diff}) + \left(\frac{K_d}{t_{diff}}\right)s \tag{13}$$

A block diagram of the control model is shown in Fig. 2. In general, we simulate the response of the system to a step change in offset error (or, analogously, particle position). We use this model to study the effect of variation of the controller parameters (K_p, K_i, K_d), and system parameters (Pe, τ_m, τ_v) on the stability of trapped particles. Using dimensionless system parameters allows us to capture the effects of a change in several dimensional parameters. For example, a variation in Peclet number can represent a change in particle diameter, a change in viscosity, a change in the strain rate, or any combination of these factors.

2 Materials and methods

2.1 Device fabrication

The hydrodynamic trap consists of a two-layer poly(dimethyl siloxane) (PDMS) device mounted on a glass coverslip, which is fabricated using standard soft-lithography techniques. The fluidic layer, which contains the sample and the six buffer channels (four inlets and two outlets), is sandwiched between a glass cover slip and the control layer. The control layer consists of an elastomeric membrane valve positioned above one of the outlet channels. The sample is flow focused at the confluence of the two inlet channels and is delivered to the center of the cross-slot junction. As described previously, pressurizing/de-pressurizing the membrane valve causes changes in the relative flow rates through the two outlets, thereby repositioning the stagnation point. In addition, the presence of a constriction in the other outlet necessitates a constant offset pressure in the valve to maintain the stagnation point at the center of the cross-slot junction. This design allows the lower outlet channel to achieve a smaller fluidic resistance than the upper outlet channel, which allows for facile control of the stagnation point position about the center of the cross-slot junction at finite pressures.
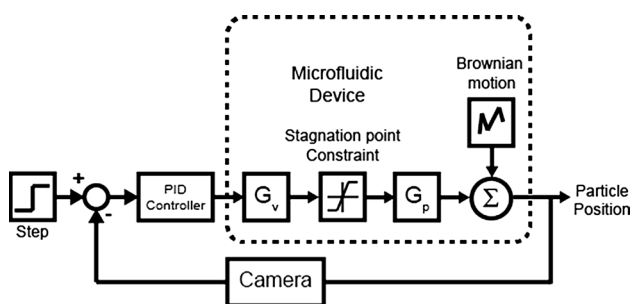

Fig. 2 Block diagram showing the control model for the trap. The model includes the stagnation point constraint, Brownian motion, and the feedback delay due to image acquisition by a camera. The *dashed box* represents the uncontrolled microfluidic device

The fluidic and control layers are individually fabricated using replica molding. For both layers, a mold is prepared by spin-coating a thin layer (~70 μm) of negative photoresist (SU-8) onto a 3″ diameter silicon wafer, followed by UV exposure using a high-resolution transparency film as a mask. Molds are then developed using propylene glycol methyl ether acetate (PGMEA). For replica molding, the PDMS-based mold layers are treated with trichloro (1H, 1H, 2H, 2H-perfluorooctyl) silane vapor to facilitate straightforward peeling and removal of the PDMS layer. The fluidic layer is fabricated by spin-coating PDMS having a 15:1 (w/w) base: crosslinker ratio, yielding a ~100 μm thick layer on the mold. The control layer is fabricated by directly pouring PDMS having a 5:1 (w/w) base: crosslinker ratio on the control layer mold. Next, both layers are partially baked at 65 °C, 12 min for the control layer and 20 min for the fluidic layer. Next, the thick control PDMS layer is peeled off, thoroughly cleaned using cleanroom tape, and then aligned and sealed onto the thin fluidic layer, followed by overnight baking at 65 °C to yield a monolithic slab. This slab is then peeled off the mold, and access holes are punched to inlets and outlets using a needle with a blunt tip. Finally, the PDMS slab is bonded to a glass coverslip using plasma oxidation to obtain a functional device.

2.2 Experimental setup

The microfluidic device is mounted on the stage of an inverted microscope (Olympus IX71) equipped with a 10× objective lens and a CCD camera. The four buffer inlets on the microdevice are connected to a single syringe mounted on a syringe pump (Harvard Apparatus) in order to maintain equal flow rates through all inlets. A separate syringe pump drives the flow for the sample inlet stream. The buffer solution is a glycerol–water solution with a viscosity of 0.0126 Pa-s at 298 K. The valve is pressurized using an electronic pressure transducer (Proportion Air) connected to a computer. A custom LabVIEW program developed for automated trapping coordinates image acquisition from the camera and regulates the pressure on the on-chip valve. The program performs the following steps: (1) acquires data from the camera to identify particles in the region of interest near the set point, (2) identifies the particle closest to the set point by comparing the distances of the particles' center of mass to the set point, (3) calculates the offset error between the set point and particle position for the selected particle, (4) calculates the current control signal (in volts) and communicates this signal with the pressure transducer to translate the position of the stagnation point, and (5) repeats this process to minimize the error in order to maintain a particle near the set point position. The image acquisition rate of the camera was 30 Hz throughout the experiments.

For estimating the control signal, we first determine whether the current voltage needs to be increased or decreased depending on the relative current positions of the stagnation point, set point, and particle position (Supplementary Information). Next, to calculate the magnitude of the change, we use a P, PI, or PD controller. The following algorithm is used for calculating the voltage for the pressure transducer:

$$\text{Err}_i = Y_i - SP$$

$$V_i = V_{i-1} \pm \left[\begin{array}{c} K_p\text{Err}_i + K_i \sum_{k=0}^{i} (\text{Err}_k \times \Delta t) \\ + \dfrac{K_d}{\Delta t}(\text{Err}_i - \text{Err}_{(i-1)}) \end{array} \right] \quad (14)$$

where Y_i is the current particle position along the extensional axis, SP is the set point, Err_i is the error between the set point and particle position, V_i is the updated voltage for the pressure transducer, K_p is the proportional gain constant, K_i is the integral gain constant, K_d is the differential gain constant, and Δt is the loop iteration time in LabVIEW, which is determined by the image acquisition rate of the camera. The loop iteration time is equal to the sum of the measurement delay and system response time. However, in our experiments, the system response time was generally small compared with the measurement delay time for a trapped particle, because minute changes in pressure are required to maintain a trapped particle near the set point. Hence, the loop iteration time reported by LabVIEW was roughly the same as the measurement delay (33 ms).

For studying the effect of the controller gains, 2.2-μm-diameter fluorescent beads (SPHERO fluorescent particles, Nile Red, Spherotech Inc., IL, USA) are trapped at specific buffer and sample flow rates and proportional gain K_p. The buffer is treated with a surfactant (0.05 % v/v Triton-X), which minimizes aggregation of the beads. Next, a series of step changes in the particle position is applied to the system, with each step having a magnitude of five pixels and a duration of 40 s. In this way, a predefined constant time period step is applied to the trapped bead for four successive steps, and its response is recorded using the LabVIEW program. Application of a series of steps for a given set of parameters allows for multiple experiments to be performed in a single run. The standard deviation of particle position in the last 10 s of each step is calculated and is used as a metric to assess trap performance and stability. The time period is chosen such that it is sufficiently larger than the characteristic diffusion time of the particle, and data toward the end of the step are generally analyzed to suppress start-up or initial transient effects in the particle trajectories. This process is used for all steps in a single run, and the mean and standard

deviation of the standard deviation values for each step in a run are calculated.

3 Results and discussion

3.1 Experimental results

3.1.1 P controller: effect of proportional gain, K_p

A proportional-only (P) controller is implemented by setting K_i and K_d to zero. For these experiments, we apply a series of periodic step changes, with each step having a magnitude of 5 pixels or ~4.95 μm and of duration 40 s. The duration of the step change was chosen to be large enough so that all the transients had damped out. During each step, we maintain a constant value of K_p and sample and buffer flow rates. Following each step change, we track the response of the trapped particle. In addition, we also vary the proportional gain K_p and monitor particle trajectories for different K_p values. Subsequently, this process is repeated for different buffer flow rates. Figure 3 shows the trajectory of a trapped particle during a series of step changes in the set point for a fixed flow rate and different values of K_p. Upon increasing the proportional gain K_p, the magnitude of position fluctuations for a trapped particle are suppressed to values smaller than the particle
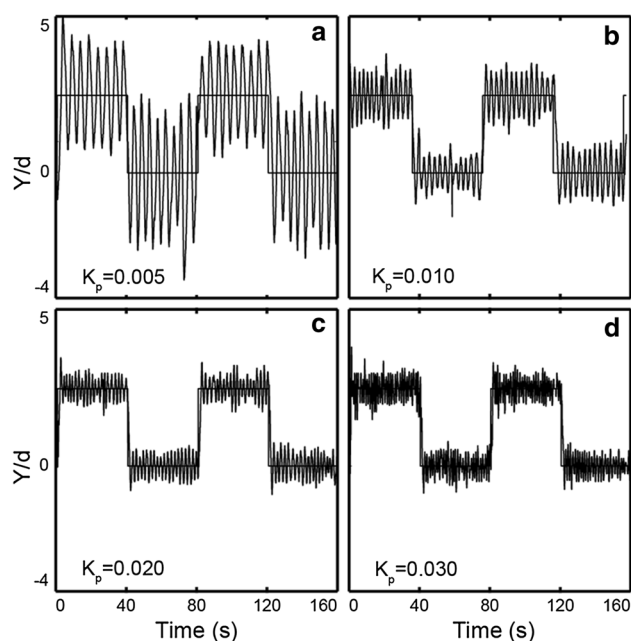

Fig. 3 Experimental trajectories of a trapped particle's position for a P controller. In all cases, a 2.2-μm-diameter particle is subjected to a step change of duration 40 s in set point position (constant flow rate of 30 and 5 μL/h for the buffer and sample, respectively). From **a** to **d**, the proportional gain was increased from 0.005 to 0.030

Fig. 4 Experimental data showing response of a trapped particle as a function of K_p and flow rate using a P controller. Standard deviation of trapped particle position is shown. The buffer flow rate is set to **a** 20 μL/h, **b** 30 μL/h, and **c** 40 μL/h
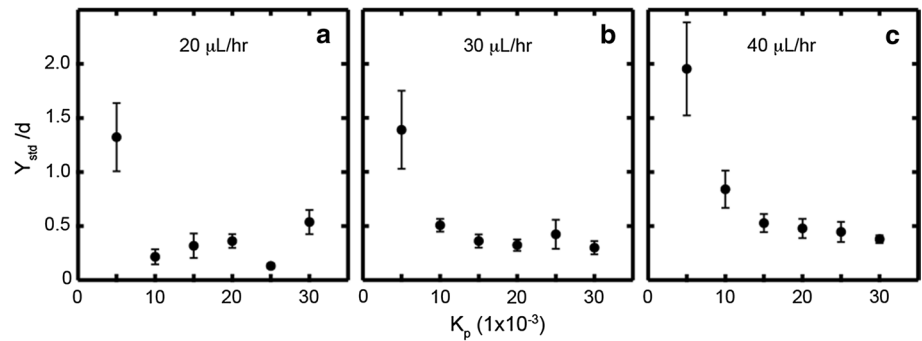

Fig. 5 Experimental data showing response of a trapped particle as a function of: **a** K_i using a PI controller with constant K_p (K_d set to 0) and **b** K_d using a PD controller with constant K_p (K_i set to 0). Standard deviation of trapped particle position is shown. The experimental parameters are: **a** sample flow rate 10 μL/h, buffer flow rate 10 μL/h, 30 s step duration; **b** sample flow rate 5 μL/h, buffer flow rate 20 μL/h, 40 s step duration
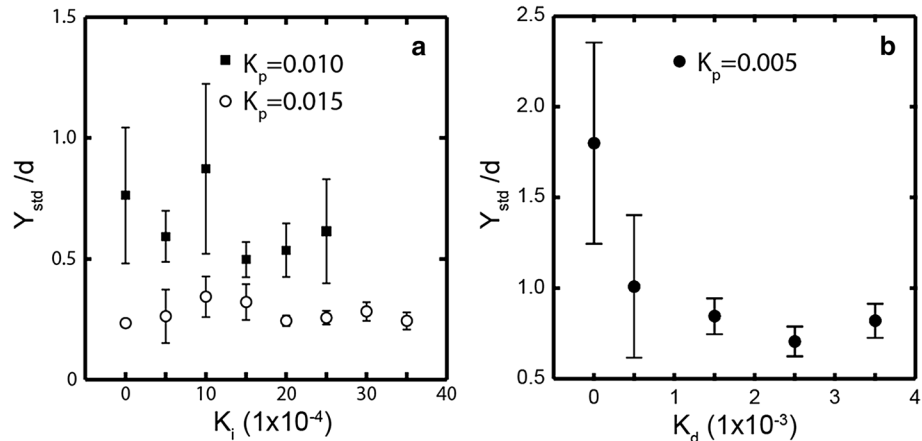
diameter (Fig. 3a–d). A video of the trapped particle corresponding to Fig. 3a has been included in the Supplementary Material.

Figure 4 shows the standard deviation of particle position as a function of proportional controller gain K_p and sample flow rate. A proportional controller accounts only for the instantaneous offset error when calculating the control signal; therefore, increasing K_p allows the stagnation point to move more aggressively in order to minimize the perturbations of a trapped particle. From Fig. 4, it is apparent that larger values of K_p result in a tighter region of confinement for a trapped particle. However, above a certain limit, further increases in K_p will overcompensate for the error, thereby resulting in particle 'ringing' oscillations. For the conditions shown in Fig. 4a, we generally observed particle 'ringing' for values of $K_p > 0.030$.

In addition, an increase in the flow rate causes a particle to be advected over larger distances in the same amount of time. Given a constant feedback rate and gain constant, it follows that the controller would need to correct for larger errors in a particle's trajectory. Therefore, for a constant controller gain K_p, the magnitude of particle position fluctuations increases upon increasing the flow rate. As shown in Fig. 4, particle position fluctuations increase in magnitude upon increasing the flow rate from 20 to 40 μL/h for small values of K_p.

3.1.2 PI controller: effect of integral gain, K_i

In a second set of experiments, we implemented a PI controller by setting $K_d = 0$ in Eq. (14). The integral gain constant K_i was varied over a fairly wide range of values for constant values of K_p and the flow rate. This process was repeated for a few sets of K_p values.

Overall, we observed that adding an integral controller does not result in an improvement in the tightness of confinement vis-à-vis a simple P controller, as shown in Fig. 5a. Upon implementing integral control and varying K_i over a range of values, the magnitude of particle position fluctuations is not improved within statistically significant values. Differences between the magnitude of fluctuations for different K_p values are primarily attributed to the increased stabilization provided by the higher K_p value alone, as evidenced in Fig. 4.

Integral controllers are commonly used to correct constant offset errors present in the control variable, which cannot be corrected by using a P controller alone. In this experiment, there is no constant offset error when a simple P controller is used. In addition, the integral term in Eq. (14) does not contribute significantly to the controller output because the standard deviation is calculated over the final 10 s of a step, when particles tend to fluctuate around the set point position. As a result, essentially no significant

improvement is observed by introducing an integral controller into this process.

3.1.3 PD controller: effect of derivative gain, K_d

We further implemented a derivative controller for the hydrodynamic trap. Here, we consider the effect of derivative gain on the stability of a trapped particle by implementing a PD controller, as shown in Fig. 5b. The derivative gain K_d was varied, while setting K_i to zero and maintaining all other parameters constant. For these experiments, we did not include integral control based on the results obtained in Fig. 5a.

We observed that derivative control greatly stabilizes the position of a trapped particle and suppresses fluctuations to within a particle diameter for smaller values of K_p. Derivative controllers account for the rate of change of error, which corresponds to the particle velocity. In stochastic systems, such as for a trapped bead subject to Brownian motion, the position of a particle at later times depends only on current conditions and is independent of the prior history (in other words, a Markov process). Consequently, a controller that modulates its signal based on particle velocity effectively damps particle fluctuations. From this view, it follows that increases in the derivative gain K_d, which acts as a damping parameter, result in decreases in particle fluctuations, as demonstrated by Fig. 5b.

On the other hand, large values of K_d can amplify noise that causes a sudden jump in particle position, such as fluctuations in the flow field. This is a significant limitation of a derivative controller, and therefore, the value of K_d should be tuned to meet the constraints dictated by noise on one hand and stability on the other. In this work, we manually varied the value of K_d, based on the response of the particle to high and low values of K_d.

Furthermore, the PD controller can be also be used to negate the effects of an increase or decrease in the temperature, which would change the magnitude of Brownian fluctuations. For example, a 5 K increase in temperature (298–303 K) would induce a 20 % increase in the root-mean-square particle displacement as a result of an increase in the thermal fluctuations of the particle and a decrease in the viscosity of the buffer solution. Under these conditions, the P and D components can be tuned separately to effectively damp particle fluctuations.

3.2 Control model and simulation results

3.2.1 Comparison with experimental results

We used a control model to further understand the performance of the hydrodynamic trap and to compare experimental results directly with the model. In the model, we
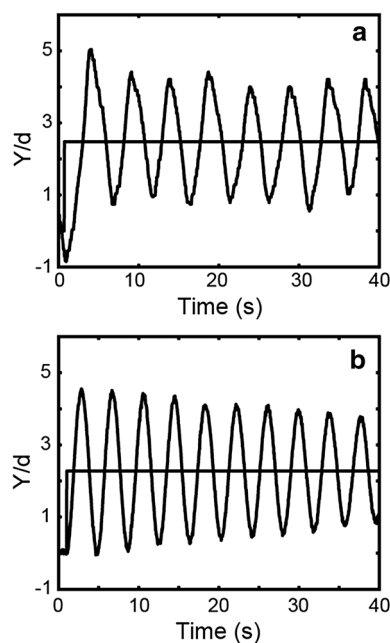

Fig. 6 Response of a 2.2-µm-trapped particle in **a** experiments and **b** simulations. In the experiment, the sample and buffer flow rates are 5 and 30 µL/h. In the simulation, $\dot{\varepsilon}^{-1} = 0.26$ s^{-1}, $K_p = -1.5$, and $K_i = -10$

set the system parameters identical to experimental conditions as described below. In the simulation, a constraint of ± 100 µm is imposed on the movement of the stagnation point, which closely captures experimental conditions. The control model is simulated using Simulink (MathWorks).

Figure 6 compares an experimental particle trajectory (Fig. 6a) to results from the simulation (Fig. 6b). This simulation result was generated by setting the particle diameter to 2.2 µm, viscosity to 0.0126 Pa-s at 298 K, and a step size of ~4.95 µm. The system response time is set to 5 ms (based on the time required to increase the pressure from 0 to 30 psi), and the measurement delay was chosen as 33 ms, which corresponds to the camera frame rate in experiments. Both experimental and simulation results show similar amplitudes of particle fluctuations, but slightly different periods, which can be attributed to different implementations of the controller in the simulation and LabVIEW. The simulation uses a controller of the form prescribed in Eq. (6), whereas the LabVIEW program uses a controller implemented according to Eq. (14). The major difference between the two versions is that the position of the stagnation point is known explicitly in the control model, whereas in experiments, the stagnation point position is generally not known in real time. For this reason, particles are trapped in experiments using knowledge of the error between the current position and set point, as well as the rate at which this error grows (see Supplementary Information). In addition, the control model has a steady
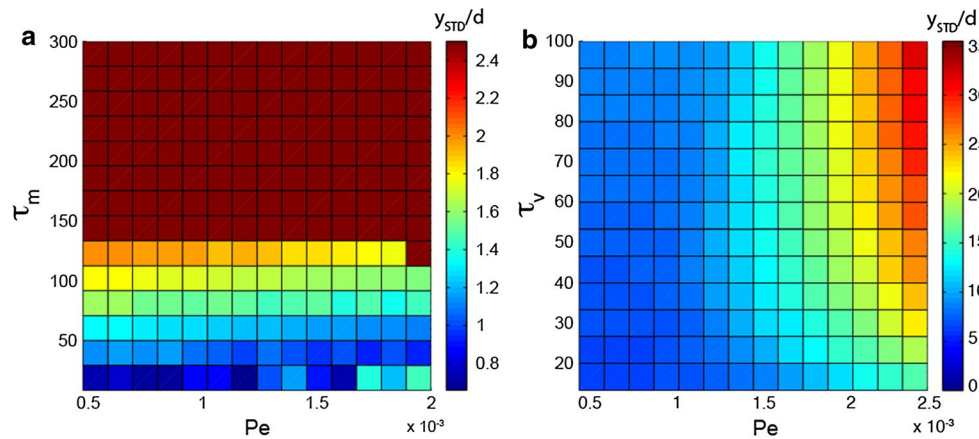
Fig. 7 Simulations showing response of a trapped particle to measurement delay, system response time, and *Pe*. **a** Heat map showing standard deviation of trapped particle position as a function of *Pe* and dimensionless measurement delay. **b** Heat map showing standard deviation of trapped particle position as a function of *Pe* and dimen-sionless system response time. The parameter values are: for calculating diffusion time: $\eta = 0.001$ Pa-s, $T = 298$ K, $d = 100$ nm, Step: 75 µm; Controller gains: $K_p = -20$, $K_i = -1.5$, $K_d = -1.4$; **a** τ_m varied from 5 to 300 with $\tau_v = 8.73$ (corresponding to 5 ms), **b** τ_v varied from 5 to 100 with $\tau_m = 57.6$ (corresponding to 33 ms)

state offset (when using a proportional-only controller) that is not present in the experiments due to the implementation of P-only control in the experimental system. We therefore added an integral control component in the control model to correct for the offset.

Using the control model, we simulated the effect of system response time τ_v, measurement delay τ_m, and particle Peclet number *Pe* on the stability of a trapped particle. Simulations were performed over a wide range of *Pe* and dimensionless measurement delays while keeping other parameters constant, and the standard deviation of the particle was determined, analogous to the procedure used for experiments.

Using this approach, we simulated the response of a small trapped particle (100 nm diameter) subjected to a large 75 µm step change in set point in a fluid of viscosity 0.001 Pa-s at 298 K (Fig. 7). In this set of simulations, we assessed the ability of the system to respond to large magnitude disturbances, such that the change in set point was 750× larger than the particle diameter. The K_p, K_i, and K_d values in the simulation are set to -20, -1.5 and -1.4, respectively. Moreover, the dimensionless measurement delay was varied between 5 and 300, and the dimensionless system response time was varied between 5 and 100, which correspond to experimental values typically encountered for image acquisition and for the system response time, respectively. It should be noted that for certain parameter ranges, the particle escaped the trap and the system was unstable; in this case, the standard deviation was set to a high value to differentiate it from stable parameter combinations (here it was set to 2.5). Finally, we also simulate the response of a trapped particle under experimental conditions (Fig. 8), with the particle diameter set to 2.2 µm, viscosity set to 0.0126 Pa-s and a step change of 4.95 µm.

3.2.2 Effect of measurement delay

For these simulations, the measurement delay was varied, while keeping the controller gains constant at the previously specified values, and the system response time set to 5 ms. Figure 7a shows a heat map illustrating trap stability (quantified as the standard deviation of particle position) as a function of *Pe* and dimensionless measurement delay τ_m. The deep red region represents parameter combinations that result in failing to trap the particle (an unstable system). The critical dimensionless measurement delay τ_m that causes a transition to instability remains constant across a wide range of particle *Pe*. Generally speaking, within the region of trap stability, the magnitude of particle fluctuations decreases upon increasing *Pe*. However, at very high *Pe*, the critical measurement delay decreases (not shown). This occurs because as the *Pe* increases, the camera needs to process image data faster to account for the increased rate of particle advection. Of course, the stability diagram shown in Fig. 7a has been generated using a specific set of values for controller gains and step change; nevertheless, we have generated similar stability diagrams using a different parameter sets, and in all cases, the qualitative trend in the variation is similar.

For further insight, we also simulate the response of a trapped particle under experimental conditions (Fig. 8a). Here, the particle position is always maintained within the accessible range of the stagnation point (i.e., particle displacement from the stagnation point is much less than 100 µm). Under these conditions, the particle is stably confined for the most of the parameter combinations; however, at high Peclet numbers and large measurement delays, an increase in particle fluctuations is observed. Thus, for small
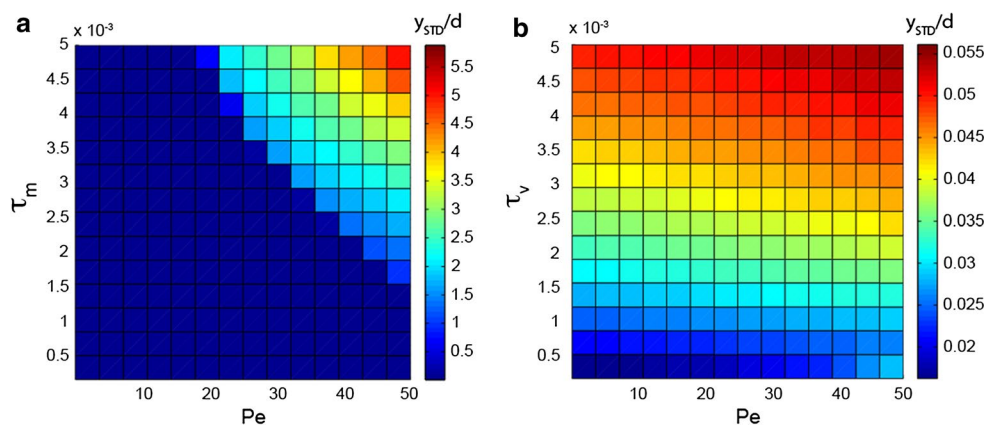
Fig. 8 Simulations showing response of a trapped particle to measurement delay, system response time, and *Pe*. **a** Heat map showing standard deviation of trapped particle position as a function of *Pe* and dimensionless measurement delay. **b** Heat map showing standard deviation of trapped particle position as a function of *Pe* and dimensionless system response time. The parameter values are: for calculating diffusion time: $\eta = 0.0126$ Pa-s, $T = 298$ K, $d = 2.2$ μm, Step $= 4.95$ μm; Controller gains: $K_p = -20$, $K_i = -1.5$, $K_d = -1.4$; **a** τ_m varied from 1×10^{-4} to 5×10^{-3} with $\tau_v = 6.5 \times 10^{-5}$ (corresponding to 5 ms), **b** τ_v varied from 1×10^{-4} to 5×10^{-3} with $\tau_m = 4.3 \times 10^{-4}$ (corresponding to 33 ms)

step change values, measurement delay becomes important only at high flow rates, and the particle trajectory is quite sensitive to large measurement delay values (standard deviation is ~5 times the particle diameter).

3.2.3 Effect of system response times

The system response time represents the time over which the trap (e.g., microfluidic device, on-chip membrane value, tubing, pressure transducer) effectively responds to changes in the stagnation point upon receiving a signal from the LabVIEW program. In the simulation, the Peclet number *Pe* and the dimensionless system response time τ_v were varied, and the particle stability was determined while maintaining other parameters such as the measurement delay (set to 33 ms) and controller gains constant.

Figure 7b shows a heat map illustrating trap stability (quantified as the standard deviation of particle position) as a function of *Pe* and system response time τ_v. Particle fluctuations increase upon increasing *Pe* at a constant system response time. Analogously, particle fluctuations also increase upon increasing the system response time at a constant *Pe*. We also observe that larger *Pe* conditions require relatively smaller system response times to maintain the same degree of particle confinement compared with lower *Pe*. Increasing both *Pe* and the system response time results in an increase in the standard deviation of particle position, as shown in the upper right corner of Fig. 7b.

Figure 8b shows a heat map of the dependence of particle standard deviation with Peclet number and system response time under experimental conditions. We note that the trend is similar to the case of large step changes such that the particle position fluctuations increase with

increasing Peclet number and system response time. Hence, for large step changes, as long as the particle is stably trapped using a suitable measurement delay, the valve response time should be reduced to smaller values in order to obtain a tighter confinement because the valve response has a strong effect on particle oscillations. On the other hand, for small step changes, we see that measurement delay is critical and needs to be small in order to minimize oscillations.

4 Conclusions

The ability to trap and manipulate individual particles is a key technology for science and engineering. To this end, the hydrodynamic trap is a simple method that allows for precise confinement of micro and nanoscale particles in free solution. In this work, we experimentally implemented and evaluated three different controllers—a proportional (P), a proportional-integral (PI), and a proportional-derivative (PD)—in order to gain an improved understanding of trap performance. We systematically investigated the effect of controller gain constants, system response times, and particle Peclet number on the stability of trapped particles.

Our results show that proportional and derivative controllers yield improvements in trap stability, quantified by tightness of confinement or the magnitude of particle fluctuations about the set point, which tend to agree with previous simulations of a related microflow process (Curtis et al. 2011). On the other hand, integral control did not improve trap stability due to the nature of the process. Thus, P and PD control enhance the stability of the trapped particle in a microfluidic hydrodynamic trap because of the different

time and length scales compared with the four-roll mill. In addition to experiments, we also developed a control model for simulating the response of the hydrodynamic trap, and we generally observed good agreement between experimental and simulation results. The control model allows for the system response and stability to be assessed over a wide range of the system parameters, including response times, measurement delay, and Peclet numbers.

Overall, our work provides an improved understanding of hydrodynamic trap stability as a function of control algorithms and system parameters, which will enable particle trapping under variable or uncertain experimental conditions (e.g., changing flow rates, solution viscosity, valve response, or image acquisition rates). In addition, the implementation of more sophisticated control algorithms can be leveraged to stabilize particle trapping under challenging experimental conditions. Improved stability will broaden the range of applications for microfluidic-based trapping, which will enable the investigation of new physical phenomena currently inaccessible using alternative methods.

As the field of microfluidics continues to mature, increasingly advanced device designs will be required for on-chip assays, materials processing, and flow metering applications. Indeed, future generations of integrated microfluidic devices will employ automated feedback controllers for fluidics or pneumatic valves to achieve these goals (Tanyeri et al. 2011b; Moyle et al. 2013). To this end, our work provides a solid framework for understanding the response of a microfluidic-based hydrodynamic trap to controller type and system parameters, which will be useful for guiding the design of next-generation, automated on-chip assays.

References

Armani MD, Chaudhary SV, Probst R, Shapiro B (2006) Using feedback control of microflows to independently steer multiple particles. J Microelectromech Syst 15:945–956. doi:10.1109/JMEMS.2006.878863

Ashkin A, Dziedzic JM, Bjorkholm JE, Chu S (1986) Observation of a single-beam gradient force optical trap for dielectric particles. Opt Lett 11:288–290

Bentley BJ, Leal LG (1986) A computer-controlled four-roll mill for investigations of particle and drop dynamics in two-dimensional linear shear flows. J Fluid Mech 167:219–240. doi:10.1017/S002211208600280X

Castelino K, Satyanarayana S, Sitti M (2005) Manufacturing of two and three-dimensional micro/nanostructures by integrating optical tweezers with chemical assembly. Robotica 23:435–439. doi:10.1017/S0263574704000864

Chiou PY, Ohta AT, Wu MC (2005) Massively parallel manipulation of single cells and microparticles using optical images. Nature 436:370–372. doi:10.1038/nature03831

Cohen AE, Moerner WE (2005) Method for trapping and manipulating nanoscale objects in solution. Appl Phys Lett. doi:10.1063/1.1872220

Cohen AE, Moerner WE (2006) Suppressing Brownian motion of individual biomolecules in solution. Proc Natl Acad Sci USA 103:4362–4365. doi:10.1073/pnas.0509976103

Cohen AE, Moerner WE (2008) Controlling Brownian motion of single protein molecules and single fluorophores in aqueous buffer. Opt Express 16:6941–6956. doi:10.1364/OE.16.006941

Cummins Z, Probst R, Shapiro B (2013) Electrokinetic tweezing: three-dimensional manipulation of microparticles by real-time imaging and flow control. Lab Chip 13:4040–4046. doi:10.1039/C3LC50674F

Curtis MD, Sheard GJ, Fouras A (2011) Feedback control system simulator for the control of biological cells in microfluidic cross slots and integrated microfluidic systems. Lab Chip 11:2343–2351. doi:10.1039/c1lc20191c

Dholakia K, Čižmár T (2011) Shaping the future of manipulation. Nat Photon 5:335–342. doi:10.1038/nphoton.2011.80

Gosse C, Croquette V (2002) Magnetic tweezers: micromanipulation and force measurement at the molecular level. Biophys J 82:3314–3329. doi:10.1016/S0006-3495(02)75672-5

Grier DG (2003) A revolution in optical manipulation. Nature 424:810–816. doi:10.1038/nature01935

Harsono MS, Zhu Q, Shi LZ et al (2013) Development of a dual joystick-controlled laser trapping and cutting system for optical micromanipulation of chromosomes inside living cells. J Biophoton 6:197–204. doi:10.1002/jbio.201200019

Juan ML, Righini M, Quidant R (2011) Plasmon nano-optical tweezers. Nat Photon 5:349–356. doi:10.1038/nphoton.2011.56

Lee H, Purdon AM, Westervelt RM (2004) Manipulation of biological cells using a microelectromagnet matrix. Appl Phys Lett 85:1063–1065. doi:10.1063/1.1776339

Lin CM, Lai YS, Liu HP et al (2008) Trapping of bioparticles via microvortices in a microfluidic device for bioassay applications. Anal Chem 80:8937–8945. doi:10.1021/ac800972t

Lutz BR, Chen J, Schwartz DT (2006) Hydrodynamic Tweezers: 1. Noncontact trapping of single cells using steady streaming microeddies. Anal Chem 78:5429–5435. doi:10.1021/ac060555y

Mcleod E, Arnold CB (2008) Subwavelength direct-write nanopatterning using optically trapped microspheres. Nat Nanotechnol 3:413–417. doi:10.1038/nnano.2008.150

Mirowski E, Moreland J, Zhang A et al (2005) Manipulation and sorting of magnetic particles by a magnetic force microscope on a microfluidic magnetic trap platform. Appl Phys Lett 86:243901. doi:10.1063/1.1947368

Moyle TM, Walker LM, Anna SL (2013) Controlling thread formation during tipstreaming through an active feedback control loop. Lab Chip 13:4534–4541. doi:10.1039/C3LC50946J

Neuman KC, Block SM (2004) Optical trapping. Rev Sci Instrum 75:2787–2809. doi:10.1063/1.1785844

Pelton M, Liu M, Kim HY et al (2006) Optical trapping and alignment of single gold nanorods by using plasmon resonances. Opt Lett 31:2075–2077. doi:10.1364/OL.31.002075

Petit T, Zhang L, Peyer KE et al (2012) Selective trapping and manipulation of microscale objects using mobile microvortices. Nano Lett 12:156–160. doi:10.1021/nl2032487

Reimann P (2002) Brownian motors: noisy transport far from equilibrium. Phys Rep 361:57–265. doi:10.1016/S0370-1573(01)00081-3

Righini M, Volpe G, Girard C et al (2008) Surface plasmon optical tweezers: tunable optical manipulation in the femtonewton range. Phys Rev Lett 100:186804. doi:10.1103/PhysRevLett.100.186804

Roxworthy BJ, Ko KD, Kumar A et al (2012) Application of plasmonic bowtie nanoantenna arrays for optical trapping, stacking, and sorting. Nano Lett 12:796–801. doi:10.1021/nl203811q

Schroeder CM, Babcock HP, Shaqfeh ESG, Chu S (2003) Observation of polymer conformation hysteresis in extensional flow. Science 301:1515–1519. doi:10.1126/science.1086070

Schroeder CM, Shaqfeh ESG, Chu S (2004) Effect of hydrodynamic interactions on DNA dynamics in extensional flow: simulation and single molecule experiment. Macromolecules 37:9242–9256. doi:10.1021/ma0494611

Tanyeri M, Schroeder CM (2013) Manipulation and confinement of single particles using fluid flow. Nano Lett 13:2357–2364. doi:10.1021/nl4008437

Tanyeri M, Johnson-Chavarria EM, Schroeder CM (2010) Hydrodynamic trap for single particles and cells. Appl Phys Lett 96:224101. doi:10.1063/1.3431664

Tanyeri M, Ranka M, Sittipolkul N, Schroeder CM (2011a) A microfluidic-based hydrodynamic trap: design and implementation. Lab Chip 11:1786–1794. doi:10.1039/C0LC00709A

Tanyeri M, Ranka M, Sittipolkul N, Schroeder CM (2011b) Microfluidic Wheatstone bridge for rapid sample analysis. Lab Chip 11:4181–4186. doi:10.1039/C1LC20604D

Tsai Y-C, Leitz K-H, Fardel R et al (2012) Parallel optical trap assisted nanopatterning on rough surfaces. Nanotechnology 23:165304. doi:10.1088/0957-4484/23/16/165304

Vorobjev IA, Liang H, Wright WH, Berns MW (1993) Optical trapping for chromosome manipulation: a wavelength dependence of induced chromosome bridges. Biophys J 64:533–538. doi:10.1016/S0006-3495(93)81398-5

Yang AHJ, Moore SD, Schmidt BS et al (2009) Optical manipulation of nanoparticles and biomolecules in sub-wavelength slot waveguides. Nature 457:71–75. doi:10.1038/nature07593